1 **FimX regulates type IV pilus localization via the Pil-Chp chemosensory system in**

2 ***Acinetobacter baylyi***

3 Taylor J. Ellison[‡1], Ian Y. Yen[‡2,3], P. Lynne Howell[2,3], Courtney K. Ellison[*1]

4 [1]Department of Microbiology, University of Georgia, Athens, GA

5 [2]Program in Molecular Medicine, Peter Gilgan Center for Research and Learning, The Hospital

6 for Sick Children, Toronto, ON M5G 0A4, Canada.

7 [3]Department of Biochemistry, University of Toronto, Toronto, ON M5S 1A8, Canada.

8 [‡]These authors contributed equally

9 *Correspondence to: c.ellison@uga.edu

10 *Running Head.* FimX regulates pilus localization

11

12 **ABSTRACT**

13 Type IV pili (T4P) are widespread dynamic appendages required for diverse prokaryotic behaviors

14 including twitching motility, biofilm formation, and DNA uptake leading to natural transformation.

15 Although the components involved in T4P assembly and dynamics are largely conserved across

16 divergent clades of bacteria, the mechanisms underlying T4P function and regulation differ

17 significantly and remain poorly characterized outside of a select few model organisms. One

18 understudied characteristic of T4P includes the spatial organization of T4P envelope-spanning

19 nanomachines and how organizational patterns contribute to single cell behaviors. The bacterial

20 species *Acinetobacter baylyi* localizes its T4P nanomachines in a unique pattern along the long

21 axis of the cell, making it a robust model to study the mechanisms underlying the regulation of

22 intracellular organization in single cell organisms. In this work, we find that the T4P regulatory

23 protein FimX has been co-opted away from regulating T4P dynamics to instead control T4P

24 positioning through a chemosensory Pil-Chp pathway. We show FimX directly interacts with the

25 Pil-Chp histidine kinase ChpA which likely influences Pil-Chp signaling and the subsequent

26   positioning of T4P machines. These data contribute to our understanding of how bacterial

27   regulatory systems can evolve to function in diverse biological processes.

28

29

30   **SIGNIFICANCE STATEMENT**

31   Subcellular organization of protein complexes plays a vital role in their function in all domains of

32   life, yet the molecular mechanisms underlying subcellular organization in bacteria remain poorly

33   understood. This work shows the T4P regulatory component FimX directly interacts with a

34   chemosensory signaling protein to regulate the positioning of T4P nanomachines. These data

35   provide insight into how signaling systems can evolve to regulate diverse processes, and they

36   establish a direct connection between environmental signaling cascades and the regulation of

37   bacterial cell biology.

38

39

40   **INTRODUCTION**

41   Many prokaryotic species encode genes to produce dynamic, filamentous appendages

42   called type IV pili (T4P) that are required for diverse behaviors including twitching motility, DNA

43   uptake leading to natural transformation, biofilm formation, and host cell adherence (Craig *et al.*,

44   2019; Ellison *et al.*, 2022b). Although T4P and related structures are broadly distributed across

45   bacteria and archaea and play an important role in single-cell lifestyles, how their production and

46   dynamics are regulated in divergent organisms remains poorly understood (Denise *et al.*, 2019).

47   T4P dynamics are essential for their function and are driven by the activity of ATP-

48   hydrolyzing motors (Craig *et al.*, 2019; McCallum *et al.*, 2019; Ellison *et al.*, 2022b). Extension

49   motors polymerize major pilin subunits that constitute the filament to drive T4P extension, while

50   retraction motors depolymerize pilins to drive T4P retraction. In many species, accessory proteins

51   and signaling molecules such as cyclic-3′,5′-dimeric guanosine monophosphate (cdG) play an

52 important role in regulating T4P dynamics and function by altering motor activity (Roberge and

53 Burrows, 2024). For example, in *Pseudomonas aeruginosa* and *Xanthomonas* spp., the small

54 protein PilZ is required for T4P production via direct interactions with the extension motor ATPase,

55 PilB (Alm *et al.*, 1996; Guzzo *et al.*, 2009). CdG also directly binds the extension motor MshE of

56 mannose-sensitive hemagglutinin (MSHA) pili found in *Vibrio cholerae*, PilF found in *Thermus*

57 *thermophilus*, and PilB in *Myxococcus xanthus* to promote motor function (Jones *et al.*, 2015;

58 Floyd *et al.*, 2020; Dye *et al.*, 2023; Neißner *et al.*, 2025). In contrast, some proteins have been

59 shown to directly inhibit extension motors in order to prevent T4P assembly as is the case with

60 the inhibition of PilB by CpiA in *Acinetobacter baylyi* or the T4P-dependent phage-encoded

61 proteins Tip, Aqs1, and Zip that inhibit T4P production in *P. aeruginosa* to prevent phage

62 reinfection (Chung *et al.*, 2014; Ellison *et al.*, 2021; Shah *et al.*, 2021; Taylor *et al.*, 2024).

63   In *Xanthomonas* and *P. aeruginosa*, the cdG-binding accessory protein FimX promotes

64 PilB extension motor activity (Guzzo *et al.*, 2009; Jain *et al.*, 2017; Llontop *et al.*, 2021). In these

65 species FimX contains degenerate diguanylate cyclase (GGDEF) and phosphodiesterase (EAL)

66 domains that do not possess in vivo enzymatic activity but retain the ability to bind cdG to regulate

67 T4P production (Guzzo *et al.*, 2009; Jain *et al.*, 2017). In *Xanthomonas* spp., FimX directly

68 interacts with PilZ to promote T4P extension, while in *P. aeruginosa*, FimX instead binds to PilB.

69 The differences between these systems highlight how accessory proteins have evolved different

70 strategies to regulate the same processes.

71   To better understand the regulatory networks underlying T4P function in different species,

72 we sought to assess the role of FimX in *A. baylyi*. Surprisingly, we found that FimX does not

73 interact with PilB nor PilZ as it does in *P. aeruginosa* or *Xanthomonas*, respectively. In line with

74 this observation, we show that FimX also does not promote T4P extension but instead has been

75 co-opted to regulate T4P localization as part of the chemosensory Pil-Chp pathway that controls

76 T4P patterning in *A. baylyi*.

77

78

RESULTS

FimX does not interact with PilB nor PilZ in *A. baylyi*

Studies in *P. aeruginosa* and *Xanthomonas* spp. suggested that FimX could interact with PilB or PilZ to regulate T4P extension in *A. baylyi*. To test direct interactions between FimX (ACIAD2209) and PilZ (ACIAD2360) or PilB (ACIAD0362), we performed bacterial adenylate cyclase two-hybrid (BACTH) assays. BACTH combinations were constructed by fusing the T25- or T18- fragments of the *Bordetella pertussis* adenylate cyclase to the N- or C- terminus of each protein, resulting in stable fusion constructs. Plate-based and quantitative β-galactosidase Miller assays revealed no direct interactions between FimX and PilB or PilZ, although a statistically significant, but modest, increase in β-galactosidase activity was detected between FimX and PilB compared to the empty vector control (Figure 1A, B, Supplementary Figure S1). To confirm that the null interactions were not due to protein expression levels, we performed Western blotting using an antibody against the T18 fragment and demonstrated that all three proteins were expressed (Supplementary Figure S2). We next wondered whether FimX may indirectly interact with PilB or PilZ, which is more easily detected by *in vivo* coimmunoprecipitation assays that can detect interactions between components within multiprotein complexes. We thus created strains encoding protein fusions *fimX-GFP* and *3xFLAG-pilB* or *3xFLAG-pilZ* for coimmunoprecipitation assays in *A. baylyi*. The *3xFLAG-pilB* allele was previously found to be fully functional by natural transformation assays (Ellison *et al.*, 2021), and the *3xFLAG-pilZ* strain was likewise able to undergo natural transformation at wildtype levels (Supplemental Figure S3). Coimmunoprecipitation assays using α-FLAG magnetic beads and 3xFLAG-PilZ or 3xFLAG-PilB as bait resulted in no FimX-GFP signal in the elution fraction, suggesting FimX does not indirectly interact with either PilZ or PilB (Figure 1C).

102

Deletion mutants lacking *fimX* make mislocalized T4P

Because FimX does not appear to regulate T4P extension via PilB or PilZ, we wondered if FimX may regulate T4P assembly via an alternative mechanism. T4P and their dynamics are required for DNA uptake leading to natural transformation, and T4P mutants defective in T4P synthesis or retraction are unable to undergo efficient natural transformation (Seitz and Blokesch, 2013; Ellison *et al.*, 2018). We thus performed natural transformation assays to assess the role of FimX in T4P production. As expected, a major pilin deletion strain ΔcomP fell below the limit of detection (Figure 2A). However, the parent strain and the ΔfimX mutant exhibited similar transformation frequencies, suggesting that FimX does not influence T4P production (Figure 2A).

Because FimX does not promote T4P synthesis, we wondered whether it may be involved in regulating another aspect of T4P function in *A. baylyi*. Previous work highlighted that wildtype *A. baylyi* produces T4P in a line along the long axis of the cell, and deletion mutants in the chemosensory Pil-Chp pathway produce T4P that are dispersed across the cell body (Ellison *et al.*, 2022a). To test whether FimX may play a role in T4P localization, we used fluorescence microscopy to image T4P in single cells. T4P can be fluorescently labeled via the introduction of a cysteine residue into the major pilin subunit for subsequent labeling with thiol-reactive maleimide dyes (Ellison *et al.*, 2017, 2019, 2021). T4P were produced at similar levels to the parent strain (Figure 2B, C), but ΔfimX mutants exhibited mislocalized or dispersed T4P (Figure 2B, D). To more easily assess T4P phenotypes, we also analyzed ΔpilT mutants lacking the retraction motor which results in retraction-deficient mutants and consequent hyperpiliation. ΔpilT strains exhibited similar phenotypes to their *pilT*-intact counterparts, confirming that FimX does not promote T4P assembly and is instead involved in regulating T4P localization (Figure 2C, D). The mislocalization of T4P in ΔfimX mutants suggests FimX participates in Pil-Chp signaling (Ellison *et al.*, 2022a).

FimX is part of the Pil-Chp chemosensory system

128   The Pil-Chp pathway shares homology to flagellar chemotaxis systems (Figure 3A) and is

129   best-characterized in *P. aeruginosa* where it regulates T4P synthesis through T4P-mediated

130   surface-sensing (Siryaporn *et al.*, 2014; Luo *et al.*, 2015; Persat *et al.*, 2015; Webster *et al.*, 2022).

131   Although the Pil-Chp pathway in *P. aeruginosa* possesses a methyl-accepting chemotaxis

132   homologue PilJ that is important for its function, PilJ is not required for T4P linear localization in

133   *A. baylyi* unlike most of the other Pil-Chp components (Ellison *et al.*, 2022a). In *P. aeruginosa*,

134   signaling from PilJ is thought to initiate phosphotransfer from the histidine kinase ChpA

135   (homologous to CheA in flagellar chemotaxis systems) to the response regulator PilG (a CheY

136   homologue), followed by further downstream signaling to induce T4P extension in response to

137   mechanical contact (Silversmith *et al.*, 2016; Kühn *et al.*, 2021). In *P. aeruginosa*, PilG is

138   connected to the T4P machinery-affiliated component FimV through the scaffolding protein FimL

139   to regulate T4P production (Inclan *et al.*, 2016). However, in *A. baylyi* these components similarly

140   interact to regulate T4P machinery localization instead of T4P extension (Ellison *et al.*, 2022a).

141   Consistent with the Pil-Chp system playing a role in T4P machinery localization, previous work

142   also showed that PilG, FimL, and FimV localize to sites of T4P synthesis in *A. baylyi* (Ellison *et*

143   *al.*, 2022a). We thus examined the localization of FimX-mRuby3 in relation to sites of T4P

144   production. Like all other FimX C-terminal fusion strains used throughout this work, FimX-mRuby3

145   was fully functional with only ~5% of cells producing dispersed T4P compared to ~55% in the

146   Δ*fimX* control (Supplemental Figure S4). Microscopy analysis revealed that FimX-mRuby3

147   localizes to the base of T4P similar to other Pil-Chp components, and approximately 90% of cells

148   with T4P exhibited colocalization between FimX-mRuby3 and labeled T4P (Figure 3B).

149   One complicating feature of the Pil-Chp system is the interdependent feedback signaling

150   between components, and the mechanism underlying this interdependency remains unclear. PilG

151   and FimL require each other to associate with FimV and both are required for FimV to linearly

152   localize along the long axis and vice versa, demonstrating that complex signaling between these

153   components is essential to establish linear T4P patterning (Ellison *et al.*, 2022a). To test whether

154   FimX may also be regulated by signaling via Pil-Chp components, we assessed FimX localization

155   in Δ*pilG*, Δ*fimL,* or Δ*fimV* mutants. As done previously, we classified localization patterns of

156   fluorescently tagged proteins into four categories: 1) long-axis localization, 2) cytoplasmically

157   diffuse signal, 3) fluorescence localized into a single punctum, or 4) multiple, fluorescent puncta

158   localized to opposite sides of the cell body (Figure 3C). In all mutants, FimX no longer localized

159   to the long axis of the cell, and instead generally exhibited cytoplasmic localization (Figure 3C,

160   D). The mislocalization of FimX also suggested that FimX may be involved in signaling to regulate

161   the localization of other Pil-Chp components. Deletion of *fimX* reduced the proportion of cells with

162   linearly positioned PilG, FimL, and FimV, supporting the model that FimX modulates the Pil-Chp

163   signal cascade (Figure 3C, E).

164

165   **_A. baylyi_ FimX functions independently of cdG and GTP**

166   A critical aspect of FimX in regulating T4P function in both *P. aeruginosa* and

167   *Xanthomonas* spp. is its ability to bind cdG via its EAL domain. A Foldseek analysis coupled with

168   AlphaFold3 prediction suggested FimX from *A. baylyi* (*Ab*FimX) exhibits similar domain

169   organization to the *P. aeruginosa* homologue (*Pa*FimX), containing degenerate CheY-like receiver

170   (REC) and Per-ARNT-Sim (PAS) domains at the N-terminus followed by a degenerate GGDEF-

171   like and EAL domains at the C-terminus (Figure 4A, Supplemental Figure S5) (Gough *et al.*, 2001;

172   Pandurangan *et al.*, 2019; Abramson *et al.*, 2024; van Kempen *et al.*, 2024). *Pa*FimX and *Ab*FimX

173   share 21% overall sequence identity and 39% sequence similarity. In *Xanthomonas*, cdG binding

174   is dependent on canonical "EAL" residues within the EAL domain, while in *P. aeruginosa* these

175   residues have diverged slightly to "EVL" but retain cdG binding with high affinity (Navarro *et al.*,

176   2009). Sequence alignment between *Pa*FimX and *Ab*FimX revealed further divergence of these

177   residues to "EVT" in *A. baylyi*, suggesting that this FimX homolog may be incapable of binding

178   cdG (Figure 4A, Supplemental Figure S6). To test whether *Ab*FimX could bind cdG, we

179   recombinantly purified FimX from both species and assessed cdG binding using isothermal

180   titration calorimetry (ITC). While *Pa*FimX bound cdG with nanomolar affinity (dissociation constant

181   K_D = 144 nM) consistent with previously reported data (Navarro *et al.*, 2009), no interaction

182   between *Ab*FimX and cdG could be detected (Figure 4B). Superimposition of the crystal structure

183   of cdG bound to the EAL domain of *Pa*FimX with the Alphafold3 predicted EAL domain of *Ab*FimX

184   highlighted drastic alterations in residues that mediate the nucleotide base including Y673, E654,

185   F652, and H533 in *Pa*FimX that diverged to S682, N663, E661, and N540 in *Ab*FimX, respectively

186   (root mean square deviation of 1.2 Å over 147 Cα atoms) (Figure 4C, Supplemental Figure S6)

187   (Navarro *et al.*, 2009). Notably, L477 of the "EVL" motif and R479 in *Pa*FimX that support the

188   phosphate ring have changed to T485 and G487, respectively, in *Ab*FimX, abrogating its ability to

189   mediate the negatively charged phosphates (Figure 4C, Supplemental Figure S6).

190   Alphafold3 predicted a GGDEF-like domain in *Ab*FimX with three rather than the typical

191   five-stranded β-sheet fold, along with divergence of the "GGDEF" sequence motif to "ENGSY"

192   upon alignment with *Pa*FimX (Figure 4A, Supplemental Figures S5, S6). Given the role of

193   GGDEF-containing proteins in synthesizing cdG from guanosine triphosphate (GTP), we

194   additionally probed for GTP binding to *Pa*FimX and *Ab*FimX using ITC and found that neither

195   protein bound GTP even at high protein concentrations (Figure 4B). Superimposition of the crystal

196   structure of GTPγS bound to the GGDEF domain of the *Caulobacter crescentus* response

197   regulator PleD (*Cc*PleD) with the AlphaFold3 predicted GGDEF-like domain from *Ab*FimX

198   revealed similarly nonconservative changes in residues that coordinate the magnesium ion and

199   GTPγS including D344, D327, and E370 of the "GGEEF" motif of *Cc*PleD to K324, M307, and

200   G349 of *Ab*FimX, respectively (root mean square deviation of 5.2 Å over 44 Cα atoms) (Figure

201   4C) (Wassmann *et al.*, 2007). In addition, the α-helix that houses R446 and K442 of *Cc*PleD to

202   mediate the γ-phosphate is truncated in *Ab*FimX and thereby missing these positively charged

203   residues (Figure 4C). Navarro and colleagues reported similar residue alterations in *Pa*FimX that

204   coordinate the magnesium ion and γ-phosphate, which explains the lack of GTP binding (Figure

205 4B) (Navarro *et al.*, 2009). Together, our biophysical and structural analyses suggest that the lack

206 of binding to cdG in *Ab*FimX further supports its functional divergence towards T4P localization.

207

cAMP signaling does not influence T4P production nor localization

209 Because of its role in Pil-Chp signaling, it is possible that other Pil-Chp signaling molecules

210 may play an important role in FimX function. In *P. aeruginosa*, Pil-Chp signaling is linked to

211 increasing cyclic adenosine monophosphate (cAMP) levels via the adenylate cyclase CyaB to

212 upregulate hundreds of genes (including those involved in T4P production) through the

213 transcriptional regulator Vfr (Fulcher *et al.*, 2010; Luo *et al.*, 2015). We thus wondered whether

214 cAMP levels or Vfr activity may regulate T4P localization via FimX in *A. baylyi*. Deletion of the

215 genes encoding either CyaB (ACIAD1397) or Vfr (ACIAD1262) in *A. baylyi* resulted in no

216 alteration in T4P localization (Figure 5A, B). Assessment of piliation similarly demonstrated no

217 change in T4P produced in Δ*cyaB* or Δ*vfr* mutants (Figure 5A, C). Together, these results

218 demonstrate that cAMP levels and Vfr-regulated genes likely do not regulate FimX function or

219 T4P production in *A. baylyi*.

220

FimX interacts with ChpA to regulate linear T4P localization via the Pil-Chp pathway

222 To identify interaction partners that could provide insight into FimX function in Pil-Chp

223 signaling, we performed a coimmunoprecipitation experiment using a functional FimX-3xFLAG

224 strain (Supplemental Figure S4) followed by mass spectrometry analysis as done previously

225 (Ellison *et al.*, 2022a). Mass spectrometry revealed a potential interaction between FimX and

226 ChpA (Supplementary Data File 1), suggesting that FimX may influence Pil-Chp signaling via the

227 ChpA sensor kinase. In support of this hypothesis, coimmunoprecipitation experiments performed

228 using ChpA-3xFLAG as the bait protein pulled down FimX (Figure 6A). To determine whether

229 ChpA and FimX directly interact, we next performed BACTH assays using plated-based and

230 quantitative β-galactosidase Miller approaches (Figure 6B, C, Supplemental Figure S7). ChpA

231 and FimX were able to directly interact in the absence of other Pil-Chp components. ChpA and

232 PilG both regulate T4P localization in *A. baylyi*, and phosphotransfer between ChpA and PilG is

233 an essential component of Pil-Chp signaling (Silversmith *et al.*, 2016). These results suggest that

234 FimX participates in the Pil-Chp pathway via direct interaction with ChpA to modulate signaling

235 required for linear T4P localization.

236

237

238 **DISCUSSION**

239   In this manuscript, we demonstrate that the accessory protein FimX has been co-opted to

240 regulate T4P localization. This is in contrast to *P. aeruginosa* where binding of FimX to PilB

241 promotes T4P extension dependent on cdG (Jain *et al.*, 2017). Our protein interaction studies in

242 *A. baylyi* demonstrated no binding between PilB and FimX, presumably due to its inability to bind

243 cdG at the EAL domain due to residue divergence (Figures 1, 4). This could explain the functional

244 divergence of FimX away from promoting T4P synthesis, consistent with the observation that

245 deletion strains of *A. baylyi fimX* retain piliation and natural transformation capabilities (Figure 2).

246 The inability of *A. baylyi* FimX to bind GTP, further suggests a shift away from cdG usage (Figure

247 4). Our finding that FimX directly interacts with ChpA and affects the localization of other Pil-Chp

248 proteins indicates participation in coordinating the Pil-Chp signaling cascade (Figures 3, 6).

249   Interestingly, FimX homologues contain a conserved REC domain that shares homology

250 to CheY, but this domain lacks the phosphorylated aspartate that is essential for signaling.

251 However, it retains the two aspartate residues at the N-terminus (In *A. baylyi* FimXD21 analogous

252 to CheYD12 and FimXD22 analogous to CheYD13) that bind metal ions essential for coordinating

253 phosphorylation (Bellsolell *et al.*, 1994). It is thus possible that the REC domain of FimX may

254 assist in coordinating phosphotransfer between Pil-Chp components or within the many

255 phosphotransfer domains found in ChpA (Silversmith *et al.*, 2016). Divergence of ChpA in *A.*

256 *baylyi* may also explain its ability to interact with FimX. *P. aeruginosa* ChpA is a large ~270 kD

257   protein compared to the relatively smaller ~160 kD ChpA in *A. baylyi*. These changes to ChpA

258   may eliminate or enable new protein interactions as is the case for FimX and ChpA reported here.

259   Although our data show that FimX in *A. baylyi* does not bind cdG, mass spectrometry

260   analysis of FimX-3xFLAG coimmunoprecipitation eluates identified a diguanylate cyclase GGDEF

261   domain-containing protein (ACIAD2242) as a potential FimX interaction partner. ACIAD2242 is

262   transcribed opposite of the secondary extension motor, TfpB, thus an alternative explanation is

263   that FimX could coordinate with another cdG-binding protein to regulate T4P-related processes.

264   Mass spectrometry analysis also identified a number of metabolism-related putative interaction

265   partners. However, interactions between these proteins and FimX require further investigation.

266   Perhaps it is not surprising that unlike in *P. aeruginosa, A. baylyi* Pil-Chp function occurs

267   independently of cAMP signaling. Previous work showed that the Pil-Chp system in *A. baylyi*

268   regulates T4P positioning rather than T4P activity as it does in *P. aeruginosa* (Ellison *et al.*,

269   2022a). Although cdG binding and cAMP regulation do not appear to be part of the Pil-Chp

270   signaling cascade in *A. baylyi*, it is possible another unidentified signaling molecule may play a

271   role in establishing T4P patterning.

272   Intriguingly, Kazmierczak *et al* suggested that aberrant FimX may result in mislocalized

273   T4P in *P. aeruginosa* (Kazmierczak *et al.*, 2006), though this study was limited by low throughput

274   imaging via electron microscopy. With the development of a broadly applicable labeling

275   methodology for imaging T4P, it is now possible to image T4P phenotypes in diverse species in

276   live cells (including *P. aeruginosa*) without cumbersome sample preparation (Ellison *et al.*, 2017,

277   2018, 2019; Koch *et al.*, 2021). Assessing T4P localization in *fimX* mutants in species with polarly

278   localized T4P such as *P. aeruginosa* and *Acinetobacter* pathogens is of significant interest, as it

279   could point to an ancestral function for FimX in regulating T4P machinery placement (Vesel and

280   Blokesch, 2021).

281   Teasing apart the exact function of FimX and the other Pil-Chp components in Pil-Chp

282   signaling remains challenging as Pil-Chp components influence each other's localization and

283 stability (Ellison *et al.*, 2022a). It is possible that multiple components participate in transient and

284 constant phosphotransfer to maintain interactions that establish linear T4P localization. The

285 localization patterns of individual Pil-Chp components in single deletion mutants may provide

286 some insight into the details of signaling. FimX became cytoplasmically diffuse in nearly 100% of

287 cells in *pilG* or *fimL* mutants, yet a *fimV* deletion resulted in half the cells showing either

288 cytoplasmically diffuse fluorescence or fluorescence localized as a single punctum (Figure 3D).

289 This suggests the nature of FimX interactions with FimV are inherently different from those with

290 PilG or FimL. It is also interesting that deletion of *pilG* or *fimL* causes the other to become

291 cytoplasmically diffuse (Ellison *et al.*, 2022a), yet they exhibit different localization patterns in *fimX*

292 mutants (Figure 3E). This may suggest a role for FimX in regulating the interplay between FimL

293 and PilG via ChpA signaling. Analysis of the reciprocal localization of all Pil-Chp component in

294 single deletion mutants is of future interest and will likely provide insight into how these

295 components interact and regulate each other, as will phosphotransfer mutations in ChpA and PilG

296 proteins.

297 The flagellar chemotaxis system in *Escherichia coli* is known for its ability to rapidly

298 regulate the direction of flagellar rotation in response to changing chemical gradients in the

299 environment (Colin *et al.*, 2021). In contrast, the placement of T4P machines is permanent and

300 takes place over much longer time scales. It is unclear why a chemosensory network would

301 regulate generationally long processes, and it is still unclear whether an environmental signal

302 exists. Previous work shows that T4P localization patterns regulate the structure of multicellular

303 communities (Ellison *et al.*, 2022a). Because multicellular communities are more resistant to

304 external stresses such as antibiotic exposure, it is probable that a stress signal may trigger

305 changes to T4P patterning to promote cell-cell aggregation. It is also possible that localized

306 signaling between individuals in the community may play a role in regulating T4P patterning to

307 adapt community structure to specific conditions.

308   Overall, this work highlights an example of how bacteria can adapt accessory proteins to

309   regulate different biological processes. The divergence of FimX away from regulating T4P

310   extension in *A. baylyi* in comparison to its relatives provides a unique platform to dissect the

311   evolution of regulatory networks and their influence on bacterial cell biology.

312

313

314   **MATERIALS AND METHODS**

315

316   **Bacterial strains, plasmids, and cloning.**

317   ***A. baylyi* strains and culture conditions.** *A. baylyi* strain ADP1 was used throughout this study.

318   For a list of strains used throughout, see Supplementary Table 1. *A. baylyi* cultures were grown

319   at 30 °C in lysogeny broth (LB) medium and on agar supplemented with kanamycin (Kan) (50

320   μg/mL), spectinomycin (60 μg/mL), gentamycin (30 μg/mL), chloramphenicol (30 μg/mL), zeocin

321   (100 μg/mL), and/or apramycin (50 μg/mL) as appropriate.

322

323   **Strain construction in *A. baylyi*.** Mutants in *A. baylyi* were made using natural transformation

324   as described previously (Ellison *et al.*, 2021, 2022a). Briefly, mutant constructs were made by

325   splicing-by-overlap (SOE) PCR to stich (1) ~3 kb of the homologous region upstream of the gene

326   of interest, (2) the mutation where appropriate (for example deletion by allelic replacement with

327   an antibiotic [AbR] cassette), and (3) ~3 kb of the homologous downstream region. For a list of

328   primers used to generate *Acinetobacter* mutants in this study, see Supplementary Table 2. The

329   upstream region was amplified using F1 + R1 primers, and the downstream region was amplified

330   using F2 + R2 primers. All AbR cassettes were amplified with ABD123

331   (ATTCCGGGGATCCGTCGAC) and ABD124 (TGTAGGCTGGAGCTGCTTC). Tagged proteins

332   were constructed using the primers indicated in Supplementary Table 2. SOE PCR reactions were

333   performed using a mixture of the upstream and downstream regions, and middle region where

334   appropriate using F1 + R2 primers. SOE PCR products were added with 50 µL of overnight-grown

335   culture to 450 µL of LB in 2-mL round-bottom microcentrifuge tubes (USA Scientific) and grown

336   at 30 °C rotating on a roller drum for 3–5 h. For AbR-constructs, transformants were serially diluted

337   and plated on LB and LB + antibiotic.

338

339   Complementation strains were constructed by placing the gene of interest under a constitutive

340   P_{tac} promoter at the *vanAB* locus as described previously (Ellison *et al.*, 2021). First, the *vanAB*

341   locus containing the Kan[R] and the constitutive P_{tac} promoter published previously (Ellison *et al.*,

342   2021) was amplified using primers CE173 + CE336 to amplify the upstream region. The

343   downstream region was amplified from the same Kan[R]-P_{tac} construct strain using primers CE406

344   + CE176. The complementation gene was then amplified using specified primers found in

345   Supplementary Table 2. SOE PCRs and natural transformations were then performed exactly as

346   described above.

347

348   Strains containing GFP tagged FimX were constructed at the *vanAB* locus linked to a Kan[R]

349   cassette for ease of moving the construct into different strains. P_{tac}-*fimX-GFP* was constructed

350   using primers CE173 + CE1747 to amplify the upstream region and primers CE2135 + CE176 to

351   amplify the downstream region from a previously constructed strain containing the

352   complementation of FimX at the *vanAB* locus (CE726). Primers CE1555 + CE1556 were used to

353   amplify GFP with designed linker sequences. SOE PCRs and natural transformations were then

354   performed exactly as described above. Strains were confirmed by Sanger sequencing using

355   designed primers indicated in Supplementary Table 2. Strains with FimX tagged at the native

356   locus with either mRuby3 or the 3xFLAG tag were also constructed using SOE PCRs with primers

357   found in Supplementary Table 2.

358

359 **Plasmid construction.** Primers used for plasmid construction in this study are listed in

360 Supplementary Table 3. Plasmids used in this study are listed in Supplementary Table 4.

361 Commercially available, chemically competent *Escherichia coli* TOP10 (Invitrogen) was used for

362 plasmid construction and was grown at 37 °C in LB supplemented with 50 µg/mL Kan or 100

363 µg/mL carbenicillin (Carb), where appropriate, for plasmid maintenance.

364

365 For construction of pET28a-derived plasmids, *fimX* from *Pseudomonas aeruginosa* PAO1 or

366 *Acinetobacter baylyi* ADP1 was PCR amplified from their respective genomic DNA and cloned

367 into pET28a plasmid with an N-terminal hexa-histidine tag using Gibson assembly (HiFi DNA

368 Assembly Master Mix; New England Biolabs). The recombinant pET28a::*fimX* vector from each

369 strain was sequence verified using whole plasmid sequencing (Plasmidsaurus).

370

371 *A. baylyi* ADP1 *fimX*, *pilB*, *pilZ*, and *chpA* were cloned into BACTH plasmids pUT18C and pUT18

372 as well as pKT25 and pKNT25, which encodes the T18 and T25 fragments of *Bordetella pertussis*

373 adenylate cyclase at the N- and C-terminal ends, respectively, using Gibson assembly (HiFi DNA

374 Assembly Master Mix; New England Biolabs). All recombinant vectors were sequence verified

375 using whole plasmid sequencing (Plasmidsaurus).

376

377 **Natural transformation assays.** Transformation assays in *A. baylyi* were performed exactly as

378 previously described (Ellison *et al.*, 2021, 2022a; Ellison and Ellison, 2024). Briefly, strains were

379 grown overnight in LB broth at 30 °C on a roller drum. Then, 50 µL of overnight culture was

380 subcultured into 450 µL of fresh LB medium and at least 50 ng of transforming DNA (tDNA) (a ~7

381 kb PCR product containing Δ*pilT*::*spec* amplified using primers CE49 + CE50) was used for all

382 transformation assays except for DNA competition assays which are detailed below. DNA was

383 quantified using a Qubit (ThermoFisher) following standard Qubit protocols. Reactions were

384 incubated with end-over-end rotation on a roller drum at 30 °C for 5 h and then plated for

385   quantitative culture on LB + antibiotic plates (to quantify transformants) and on plain LB plates (to

386   quantify total viable counts). Data are reported as the transformation frequency, which is defined

387   as the (CFU/mL of transformants) / (CFU/mL of total viable counts).

388

389   **Pilin labeling, imaging, and quantification.** Pilin labeling in *A. baylyi* was performed as

390   described previously (Ellison *et al.*, 2022a; Ellison and Ellison, 2024). Briefly, 100 µL of overnight

391   cultures was added to 900 µL of fresh LB in a 1.5 mL microcentrifuge tube, and cells were grown

392   at 30 °C rotating on a roller drum for 70 min. Cells were then centrifuged at 18,000 x g for 1 min

393   and resuspended in 50 µL of LB before labeling with 25 µg/mL of AlexaFluor488 C5-maleimide

394   (AF488-mal) (ThermoFisher) for 15 min at room temperature. Labeled cells were centrifuged,

395   washed three times with 100 µL of PBS and resuspended in 5–40 µL PBS. Cell bodies were

396   imaged using phase-contrast microscopy while labeled pili were imaged using fluorescence

397   microscopy on a Nikon Ti2-E microscope using a Plan Apo 100X oil immersion objective, a

398   GFP/FITC/Cy2 filter set for pili, a Hamamatsu ORCA-Fusion Gen-III cCMOS camera, and Nikon

399   NIS Elements Imaging Software. Cell numbers and the percent of cells making pili were quantified

400   manually using Fiji. All imaging was performed under 1% agarose pads made with PBS solution.

401

402   **FimX imaging and quantification.** 100 µL of overnight FimX-mRuby3 culture was added to 900

403   µL of fresh LB in a 1.5 mL microcentrifuge tube, and cells were grown at 30 °C rotating on a roller

404   drum for 70 min. Cells were then centrifuged at 18,000 x g for 1 min and resuspended in 5-40 µL

405   of PBS. Cell bodies were imaged using phase-contrast microscopy while labeled FimX were

406   imaged using fluorescence microscopy on a Nikon Ti2-E microscope using a Plan Apo 100X oil

407   immersion objective, a DSRed/TRITC/Cy3 filter set for labeled FimX, a Hamamatsu ORCA-

408   Fusion Gen-III cCMOS camera, and Nikon NIS Elements Imaging Software. Cell numbers and

409   the localization of FimX were quantified manually using Fiji. All imaging was performed under 1%

410   agarose pads made with PBS solution.

411

412   **Coimmunoprecipitation assays.** Coimmunoprecipitation experiments were performed as

413   described previously (Ellison *et al.*, 2021), with some differences. Cultures of cells were grown

414   shaking overnight either in 3 ml LB in 14 ml culture tubes at 30 °C or in 50 ml LB in 250 ml volume

415   flasks at 30 °C. Overnight cultures of cells grown in tubes in LB medium were diluted by 1/10 into

416   fresh LB for a total volume 50 mL in 250 mL volume flasks. Then 50 mL cultures were grown to

417   exponential growth phase by shaking for 1.5 h at 30 °C. Overnight cultures grown shaking

418   overnight were not placed into exponential. The total culture volume was then harvested at

419   10,000 × g for 10 min at room temperature, and the supernatant was removed. Cell pellets were

420   resuspended in 2 ml of Buffer 1 (50 mM Tris-HCl pH 7.4, 150 mM NaCl, 1 mM EDTA) and

421   transferred to 2 ml volume microcentrifuge tubes and centrifuged at 10,000 × g for 3 min. Cells

422   were washed once more with 2 ml of Buffer 1, and washed pellets were resuspended in 1 ml of

423   Buffer 2 (50 mM Tris-HCl pH 7.4, 150 mM NaCl, 1 mM EDTA, 10 mM $MgCl_2$, 0.1% Triton X-100,

424   2% v/v glycerol). To lyse cells, 30 units of DNase I (New England Biolabs) and 10 µl of

425   concentrated protease inhibitor cocktail (Sigma) (one pellet dissolved in 500 µl of ddH2O) were

426   added to cell suspensions and sonicated using a 418 ultrasonic cell disruptor microtip probe

427   (Misonix). Cell debris was removed by centrifugation at 10,000 × g for 5 min at 4 °C. 50 µl of cell

428   lysates was added to a fresh 1.7 ml centrifuge tube and set aside for input analysis. 50 µl aliquots

429   of α-FLAG magnetic bead slurry (Sigma) in 1.5 ml microcentrifuge tubes were washed three times

430   with 1 ml of Buffer 2 using a magnetic collection stand. Up to 1 ml of cell lysates was added to

431   washed magnetic beads and subjected to end-over-end rotation at 4 °C for 2 h. Beads were then

432   washed three times with 0.5 ml of Buffer 2, with 10 min incubations in Buffer 2 at 4 °C between

433   each wash step. Beads were briefly washed a 4th time with 0.5 ml Buffer 2. To elute proteins from

434   α-FLAG beads, 100 µl of elution buffer (150 µg/ml 3X-FLAG peptide, Sigma, in Buffer 2) was

435   added and samples were subjected to end-over-end rotation at 4 °C for 30 min. Eluates were

436   mixed with 4X SDS running buffer (40% v/v glycerol, 250 mM Tris-HCl pH 6.8, 0.8% w/v

437   bromophenol blue, 20% v/v β-mercaptoethanol, 8% w/v SDS) and heated to 100 °C for 10–15 min

438   before separation on a 4–20% pre-cast SDS-PAGE gel (BioRad) for ~15 min so that the total

439   protein was contained in the top ~1 cm of the gel. Using a new razor blade, the gel was cut to

440   contain only the samples and the protein ladder. Then, a western blot analysis was performed on

441   the gel according to the protocol below.

442

443   **Western blotting of coimmunoprecipitation assay products**. After proteins were separated

444   on a 4–20% pre-cast polyacrylamide gel (Biorad) by SDS electrophoresis according to the

445   coimmunoprecipitation protocol previously described, protein bands were electrophoretically

446   transferred to a nitrocellulose membrane, and probed with 1:5000 dilution of mouse monoclonal

447   α-FLAG antibodies (Sigma) and a 1:2500 dilution of mouse monoclonal α-GFP (Roche

448   Diagnostics) primary antibodies. Blots were washed and then probed with a 1:10,000 dilution of

449   goat α-mouse antibody conjugated to horse radish peroxidase (Sigma). Blots were then incubated

450   with SuperSignal West Pico PLUS Chemiluminescence substrate (ThermoFisher) and then

451   imaged using a BioRad Chemidoc imaging system.

452

453   **Mass spectrometry.** Mass spectrometry analysis was performed as done previously (Ellison *et*

454   *al.*, 2022a). In-gel digestion of protein bands using trypsin was performed as in Shevchenko *et al*.

455   (Shevchenko *et al.*, 2007). Trypsin digested samples were dried completely in a SpeedVac and

456   resuspended with 20 µl of 0.1% formic acid pH 3 in water. 2 µl (~360 ng) was injected per run

457   using an Easy-nLC 1200 UPLC system. Samples were loaded directly onto a 45 cm long 75 µm

458   inner diameter nano capillary column packed with 1.9 µm C18-AQ resin (Dr. Maisch, Germany)

459   mated to metal emitter in-line with an Orbitrap Fusion Lumos (Thermo Scientific, USA). Column

460   temperature was set at 45 ºC and two-hour gradient method with 300 nl per minute flow was used.

461   The mass spectrometer was operated in data dependent mode with the 120,000 resolution MS1

462   scan (positive mode, profile data type, AGC gain of 4e5, maximum injection time of 54 s and mass

463   range of 375-1500 m/z) in the Orbitrap followed by HCD fragmentation in ion trap with 35%

464   collision energy. Dynamic exclusion list was invoked to exclude previously sequenced peptides

465   for 60 s and maximum cycle time of 3 s was used. Peptides were isolated for fragmentation using

466   quadrupole (1.2 m/z isolation window). Ion-trap was operated in Rapid mode.

467

468   Raw files were searched using Byonic (Bern *et al.*, 2012) and Sequest HT algorithms (Eng *et al.*,

469   1994) within the Proteome Discoverer 2.2 suite (Thermo Scientific, USA). 10 ppm MS1 and 0.4

470   Da MS2 mass tolerances were specified. Carbamidomethylation of cysteine was used as fixed

471   modification, oxidation of methionine, deamidation of asparagine and glutamine were specified

472   as dynamic modifications. Pyro glutamate conversion from glutamic acid and glutamine are set

473   as dynamic modifications at peptide N-terminus. Acetylation was specified as dynamic

474   modification at protein N-terminus. Trypsin digestion with maximum of two missed cleavages were

475   allowed. Files were searched against UP000000430 *Acinetobacter baylyi* database downloaded

476   from Uniprot.org.

477

478   Scaffold (version Scaffold_4.11.1, Proteome Software Inc., Portland, OR) was used to validate

479   MS/MS based peptide and protein identifications. Peptide identifications were accepted if they

480   could be established at greater than 95.0% probability by the Scaffold Local FDR algorithm.

481   Protein identifications were accepted if they could be established at greater than 99.9% probability

482   and contained at least 2 identified peptides. Protein probabilities were assigned by the Protein

483   Prophet algorithm (Nesvizhskii *et al.*, 2003).

484

485   **FimX Expression and Purification.** *E. coli* BL21 CodonPlus (DE3) cells were transformed with

486   pET28a::*fimX* from *P. aeruginosa* or *A. baylyi* and grown in 2 L of LB containing 50 µg/mL of Kan

487   at 37 °C to an OD_{600} of 0.6-0.8. Protein expression was induced by the addition of isopropyl-D-1-

488   thiogalactopyranoside (IPTG) to a final concentration of 0.1 mM for 18 hours at 18°C. Cells were

489   harvested by centrifugation at 7000 x g for 15 mins. Pellets were resuspended in 40 mL of binding

490   buffer (50 mM HEPES, pH 8, 300 mM NaCl, 10% v/v glycerol, 30 mM imidazole) in addition to a

491   protease inhibitor cocktail tablet (SIGMA*FAST*™, EDTA-free), and small amounts of powdered

492   lysozyme (Bio Basic) and DNase I (Bio Basic). Cell lysis was performed by passage through an

493   Emulsiflex-c3 homogenizer and insoluble cell debris was clarified by centrifugation at 35,000 x g

494   for 45 mins. Filtered supernatant was incubated with 2.5 mL of Ni-NTA agarose resin (Qiagen)

495   pre-equilibrated with binding buffer. The column was washed with 75 mL of the same buffer before

496   elution in 25 mL of elution buffer (binding buffer plus 300 mM imidazole). The sample was

497   concentrated using an Amicon Ultra-15 centrifugal device (Millipore) with 100 kDa molecular

498   weight cut-off at 4000 x g in ten-minute intervals and subsequently injected into a HiLoad 16/60

499   Superdex 200 prep grade gel filtration column (GE Healthcare) pre-equilibrated in SEC buffer (50

500   mM HEPES, pH 8, 200 mM NaCl, 10% v/v glycerol) for further purification. Fractions containing

501   FimX were assessed by 12% SDS-PAGE gel, concentrated, and flash frozen in liquid nitrogen for

502   storage at -80°C until use.

503

504   **Isothermal Titration Calorimetry.** Cyclic di-guanosine monophosphate (cdG) (InvivoGen) (250

505   µM in the syringe) and *Pa*FimX or *Ab*FimX proteins (25 µM in the cell) were prepared in SEC

506   buffer. Guanosine triphosphate (GTP) (Sigma) (1 mM in the syringe) and FimX proteins (100 µM

507   in the cell) were prepared in SEC buffer plus 10 mM $MgCl_2$. Calorimetric titrations were conducted

508   using a MicroCal PEAQ-ITC Automated microcalorimeter (Malvern Panalytical) at 25°C,

509   comprising 19 2-µL injections of 4 s per injection with 120 s intervals between injections. The first

510   titration was 0.4 µL for 0.8 s. The MicroCal PEAQ-ITC software v.1.41 (Malvern Panalytical) was

511   used to subtract the heats of dilution for titrating cdG or GTP into buffer from the sample and to

512   perform curve-fitting using a single-site binding model to derive the dissociation constant.

513

514 **Bacterial Adenylate Cyclase Two-Hybrid (BACTH) Assays.** Combinations of the *A. baylyi*

515 FimX and PilB or PilZ or ChpA T18 and T25 fusion proteins were transformed into *E. coli* BTH101

516 (Euromedex). Overnight cultures of each combination were inoculated with 5 mL of LB

517 supplemented with 50 µg/mL of Kan, 100 µg/mL of Carb, and 0.5 mM of IPTG and grown overnight

518 at 30 °C for 18-20 hours. For the plates showing all combinations or the plates that complemented

519 the quantitative Miller assay, 5 or 10 µL, respectively, of overnight cultures was spotted onto LB

520 agar plate containing 50 µg/mL of Kan, 100 µg/mL of Carb, 0.5 mM of IPTG, and 50 µg/mL of 5-

521 bromo-4-chloro-3-indolyl-β-D-galactopyranoside (X-Gal). Plates were incubated at 30 °C for 48

522 hours and subsequently at 4 °C for 24 hours prior to imaging. pUT18C::zip and pKT25::zip vector

523 pairs and empty pUT18C and pKT25 vector pairs were used as positive and negative controls,

524 respectively.

525

526 A β-galactosidase Miller assay was performed to quantify the strength of the BACTH interactions.

527 Overnight cultures grown in 5 mL LB supplemented with 50 µg/mL of Kan, 100 µg/mL of Carb,

528 and 0.5 mM of IPTG at 30 °C for 20 hours were normalized to an OD_{600} of 1 in a 1 mL volume

529 and centrifuged at 12,000 rpm for 5 mins. Cell pellets were resuspended in 500 µL of 60 mM

530 Na_2HPO_4, 40 mM NaH_2PO_4, pH 7, 20 mM KCl, 2 mM $MgSO_4$, 0.4 mg/mL sodium deoxycholate,

531 0.8 mg/mL cetyltrimethylammonium bromide, and 75 mM β-mercaptoethanol and incubated at 30

532 °C for 30 mins. 200 µL of cellular material was mixed with 600 µL of 60 mM Na_2HPO_4, 40 mM

533 NaH_2PO_4, pH 7, and 1 mg/mL ortho-nitrophenyl-β-galactoside and incubated at 30 °C for 20 mins.

534 700 µL of 1 M Na_2CO_3 solution was added to stop the reaction and centrifuged for 10 mins. 200

535 µL of each reaction was measured in a 96-well plate in triplicates at absorbances of 420 nm and

536 550 nm. β-galactosidase activity in Miller units was calculated using the following equation: $[A_{420}$

537 $- (1.75 \times A_{550})]$ / (reaction time in minutes x OD_{600} x volume of reaction assayed in mL) x 1000.

538

539 **Western Blotting of BACTH constructs.** Overnight cultures grown in 5 mL LB supplemented

540 with 50 µg/mL of Kan, 100 µg/mL of Carb, and 0.5 mM of IPTG at 30 °C for 20 hours were

541 normalized to an OD_{600} of 1 in a 1 mL volume. Cells were pelleted by centrifugation at 15,000 rpm

542 for 5 mins. After removing the supernatant, cell pellets were resuspended in 100 µL of 2× Laemmli

543 buffer, boiled for 20 mins, and separated by SDS-PAGE using 12% gels. Protein bands were

544 transferred to 0.2-µm PVDF membrane (25 V, 1.5 hours) with Towbin buffer (25 mM Tris-HCl, pH

545 8.6, 192 mM glycine, 20% v/v methanol) and blocked in 5% (w/v) skim milk powder resuspended

546 in Tris buffered saline with Tween-20 (TBS-T; 20 mM Tris-HCl pH 7.6, 150 mM NaCl, 0.05% v/v

547 Tween-20) for 1 hour. Membranes were probed with α-adenylate cyclase toxin mouse monoclonal

548 antibodies (Santa Cruz Biotechnology) at 1:5000 dilution in 1% (w/v) skim milk powder

549 resuspended in TBS-T for 20 hours. Membranes were then washed four times with TBS-T and

550 probed with horseradish peroxidase (HRP)-conjugated goat anti-mouse antibody (Biorad) at

551 1:3000 dilution in 1% (w/v) skim milk powder resuspended in TBS-T for 1 hour. Membranes were

552 washed three times with TBS-T and developed using SuperSignal West Pico Plus

553 chemiluminescent substrate (ThermoFisher Scientific).

554

565

566

567

REFERENCES

Abramson, J, Adler, J, Dunger, J, Evans, R, Green, T, Pritzel, A, Ronneberger, O, Willmore, L, Ballard, AJ, Bambrick, J, *et al.* (2024). Accurate structure prediction of biomolecular interactions with AlphaFold 3. Nature 630, 493–500.

Alm, RA, Bodero, AJ, Free, PD, and Mattick, JS (1996). Identification of a novel gene, pilZ, essential for type 4 fimbrial biogenesis in Pseudomonas aeruginosa. J Bacteriol 178, 46–53.

Bellsolell, L, Prieto, J, Serrano, L, and Coll, M (1994). Magnesium Binding to the Bacterial Chemotaxis Protein CheY Results in Large Conformational Changes Involving its Functional Surface. Journal of Molecular Biology 238, 489–495.

Bern, M, Kil, YJ, and Becker, C (2012). Byonic: Advanced peptide and protein identification software. Current Protocols in Bioinformatics Chapter 13.

Chung, IY, Jang, HJ, Bae, HW, and Cho, YH (2014). A phage protein that inhibits the bacterial ATPase required for type IV pilus assembly. Proceedings of the National Academy of Sciences of the United States of America 111, 11503–11508.

Colin, R, Ni, B, Laganenka, L, and Sourjik, V (2021). Multiple functions of flagellar motility and chemotaxis in bacterial physiology. FEMS Microbiol Rev 45, fuab038.

Craig, L, Forest, KT, and Maier, B (2019). Type IV pili: dynamics, biophysics and functional consequences. Nature Reviews Microbiology, 1.

Denise, R, Abby, SS, and Rocha, EPC (2019). Diversification of the type IV filament superfamily into machines for adhesion, protein secretion, DNA uptake, and motility. PLOS Biology 17, e3000390.

Dye, KJ, Salar, S, Allen, U, Smith, W, and Yang, Z (2023). Myxococcus xanthus PilB interacts with c-di-GMP and modulates motility and biofilm formation. Journal of Bacteriology 205, e00221-23.

Ellison, CK, Dalia, TN, Dalia, AB, and Brun, YV (2019). Real-time microscopy and physical perturbation of bacterial pili using maleimide-conjugated molecules. Nature Protocols 14.

Ellison, CK, Dalia, TN, Klancher, CA, Shaevitz, JW, Gitai, Z, and Dalia, AB (2021). Acinetobacter baylyi regulates type IV pilus synthesis by employing two extension motors and a motor protein inhibitor. Nat Commun 12, 3744.

599 Ellison, CK, Dalia, TN, Vidal Ceballos, A, Wang, JC-Y, Biais, N, Brun, YV, and Dalia, AB
600 (2018). Retraction of DNA-bound type IV competence pili initiates DNA uptake during
601 natural transformation in Vibrio cholerae. Nature Microbiology 3, 773–780.

602 Ellison, CK, Fei, C, Dalia, TN, Wingreen, NS, Dalia, AB, Shaevitz, JW, and Gitai, Z
603 (2022a). Subcellular localization of type IV pili regulates bacterial multicellular
604 development. Nat Commun 13, 6334.

605 Ellison, CK, Kan, J, Dillard, RS, Kysela, DT, Ducret, A, Berne, C, Hampton, CM, Ke, Z,
606 Wright, ER, Biais, N, *et al.* (2017). Obstruction of pilus retraction stimulates bacterial
607 surface sensing. Science 358, 535–538.

608 Ellison, CK, Whitfield, GB, and Brun, YV (2022b). Type IV Pili: dynamic bacterial
609 nanomachines. FEMS Microbiology Reviews 46, fuab053.

610 Ellison, TJ, and Ellison, CK (2024). DNA binding is rate-limiting for natural
611 transformation. 2024.06.06.597730.

612 Eng, JK, McCormack, AL, and Yates, JR (1994). An approach to correlate tandem mass
613 spectral data of peptides with amino acid sequences in a protein database. Journal of
614 the American Society for Mass Spectrometry 5, 976–989.

615 Floyd, KA, Lee, CK, Xian, W, Nametalla, M, Valentine, A, Crair, B, Zhu, S, Hughes, HQ,
616 Chlebek, JL, Wu, DC, *et al.* (2020). c-di-GMP modulates type IV MSHA pilus retraction
617 and surface attachment in Vibrio cholerae. Nature Communications 11, 1–16.

618 Fulcher, NB, Holliday, PM, Klem, E, Cann, MJ, and Wolfgang, MC (2010). The
619 Pseudomonas aeruginosa Chp chemosensory system regulates intracellular cAMP
620 levels by modulating adenylate cyclase activity. Molecular Microbiology 76, 889–904.

621 Gough, J, Karplus, K, Hughey, R, and Chothia, C (2001). Assignment of homology to
622 genome sequences using a library of hidden Markov models that represent all proteins
623 of known structure. J Mol Biol 313, 903–919.

624 Guzzo, CR, Salinas, RK, Andrade, MO, and Farah, CS (2009). PILZ protein structure
625 and interactions with PILB and the FIMX EAL domain: implications for control of type IV
626 pilus biogenesis. J Mol Biol 393, 848–866.

627 Inclan, YF, Persat, A, Greninger, A, Von Dollen, J, Johnson, J, Krogan, N, Gitai, Z, and
628 Engel, JN (2016). A scaffold protein connects type IV pili with the Chp chemosensory
629 system to mediate activation of virulence signaling in Pseudomonas aeruginosa.
630 Molecular Microbiology 101, 590–605.

631 Jain, R, Sliusarenko, O, and Kazmierczak, BI (2017). Interaction of the cyclic-di-GMP
632 binding protein FimX and the Type 4 pilus assembly ATPase promotes pilus assembly.
633 PLOS Pathogens 13, e1006594.

634 Jones, CJ, Utada, A, Davis, KR, Thongsomboon, W, Zamorano Sanchez, D, Banakar, V,
635 Cegelski, L, Wong, GCL, Yildiz, FH, Sanchez, DZ, *et al.* (2015). C-di-GMP regulates
636 motile to sessile transition by modulating MshA pili biogenesis and near-surface motility
637 behavior in Vibrio cholerae. PLoS Pathog 11, e1005068.

638 Kazmierczak, BI, Lebron, MB, and Murray, TS (2006). Analysis of FimX, a
639 phosphodiesterase that governs twitching motility in Pseudomonas aeruginosa.
640 Molecular Microbiology 60, 1026–1043.

641 van Kempen, M, Kim, SS, Tumescheit, C, Mirdita, M, Lee, J, Gilchrist, CLM, Söding, J,
642 and Steinegger, M (2024). Fast and accurate protein structure search with Foldseek.
643 Nat Biotechnol 42, 243–246.

644 Koch, MD, Fei, C, Wingreen, NS, Shaevitz, JW, and Gitai, Z (2021). Competitive binding
645 of independent extension and retraction motors explains the quantitative dynamics of
646 type IV pili. Proc Natl Acad Sci U S A 118, e2014926118.

647 Kühn, MJ, Talà, L, Inclan, YF, Patino, R, Pierrat, X, Vos, I, Al-Mayyah, Z, Macmillan, H,
648 Negrete, J, Engel, JN, *et al.* (2021). Mechanotaxis directs Pseudomonas aeruginosa
649 twitching motility. Proceedings of the National Academy of Sciences 118, e2101759118.

650 Llontop, EE, Cenens, W, Favaro, DC, Sgro, GG, Salinas, RK, Guzzo, CR, and Farah,
651 CS (2021). The PilB-PilZ-FimX regulatory complex of the Type IV pilus from
652 Xanthomonas citri. PLOS Pathogens 17, e1009808.

653 Luo, Y, Zhao, K, Baker, AE, Kuchma, SL, Coggan, KA, Wolfgang, MC, Wong, GC, and
654 O'Toole, GA (2015). A hierarchical cascade of second messengers regulates
655 Pseudomonas aeruginosa surface behaviors. mBio 6.

656 McCallum, M, Burrows, LL, and Howell, PL (2019). The Dynamic Structures of the Type
657 IV Pilus. Microbiology Spectrum 7, 10.1128/microbiolspec.psib-0006–2018.

658 Navarro, MVAS, De, N, Bae, N, Wang, Q, and Sondermann, H (2009). Structural
659 Analysis of the GGDEF-EAL Domain-Containing c-di-GMP Receptor FimX. Structure
660 17, 1104–1116.

661 Neißner, K, Keller, H, Kirchner, L, Düsterhus, S, Duchardt-Ferner, E, Averhoff, B, and
662 Wöhnert, J (2025). The structural basis for high-affinity c-di-GMP binding to the GSPII-B
663 domain of the traffic ATPase PilF from *Thermus thermophilus*. Journal of Biological
664 Chemistry 301, 108041.

665 Nesvizhskii, AI, Keller, A, Kolker, E, and Aebersold, R (2003). A statistical model for
666 identifying proteins by tandem mass spectrometry. Analytical Chemistry 75, 4646–4658.

667 Pandurangan, AP, Stahlhacke, J, Oates, ME, Smithers, B, and Gough, J (2019). The
668 SUPERFAMILY 2.0 database: a significant proteome update and a new webserver.
669 Nucleic Acids Research 47, D490–D494.

670 Persat, A, Inclan, YF, Engel, JN, Stone, HA, and Gitai, Z (2015). Type IV pili
671 mechanochemically regulate virulence factors in *Pseudomonas aeruginosa*.
672 Proceedings of the National Academy of Sciences 112, 7563–7568.

673 Roberge, NA, and Burrows, LL (2024). Building permits—control of type IV pilus
674 assembly by PilB and its cofactors. Journal of Bacteriology 206, e00359-24.

675 Seitz, P, and Blokesch, M (2013). DNA-uptake machinery of naturally competent Vibrio
676 cholerae. Proceedings of the National Academy of Sciences of the United States of
677 America 110, 17987–17992.

678 Shah, M, Taylor, VL, Bona, D, Tsao, Y, Stanley, SY, Pimentel-Elardo, SM, McCallum, M,
679 Bondy-Denomy, J, Howell, PL, Nodwell, JR, *et al.* (2021). A phage-encoded anti-
680 activator inhibits quorum sensing in Pseudomonas aeruginosa. Molecular Cell.

681 Shevchenko, A, Tomas, H, Havliš, J, Olsen, J V., and Mann, M (2007). In-gel digestion
682 for mass spectrometric characterization of proteins and proteomes. Nature Protocols 1,
683 2856–2860.

684 Silversmith, RE, Wang, B, Fulcher, NB, Wolfgang, MC, and Bourret, RB (2016).
685 Phosphoryl Group Flow within the *Pseudomonas aeruginosa* Pil-Chp Chemosensory
686 System. Journal of Biological Chemistry 291, 17677–17691.

687 Siryaporn, A, Kuchma, SL, O'Toole, GA, Gitai, Z, O'Toole, GA, and Gitai, Z (2014).
688 Surface attachment induces Pseudomonas aeruginosa virulence. Proceedings of the
689 National Academy of Sciences 111, 16860–16865.

690 Taylor, VL, Shah, M, Patel, PH, Yusuf, A, Burk, CM, Gitai, Z, Davidson, AR, Koch, MD,
691 and Maxwell, KL (2024). Prophages block cell surface receptors to ensure survival of
692 their viral progeny. 2024.03.05.583538.

693 Vesel, N, and Blokesch, M (2021). Pilus production in Acinetobacter baumannii is
694 growth phase dependent and essential for natural transformation. Journal of
695 Bacteriology 203.

696 Wassmann, P, Chan, C, Paul, R, Beck, A, Heerklotz, H, Jenal, U, and Schirmer, T
697 (2007). Structure of BeF3−-Modified Response Regulator PleD: Implications for
698 Diguanylate Cyclase Activation, Catalysis, and Feedback Inhibition. Structure 15, 915–
699 927.

700 Webster, SS, Mathelié-Guinlet, M, Verissimo, AF, Schultz, D, Viljoen, A, Lee, CK,
701 Schmidt, WC, Wong, GCL, Dufrêne, YF, and O'Toole, GA (2022). Force-Induced
702 Changes of PilY1 Drive Surface Sensing by Pseudomonas aeruginosa. mBio 13,
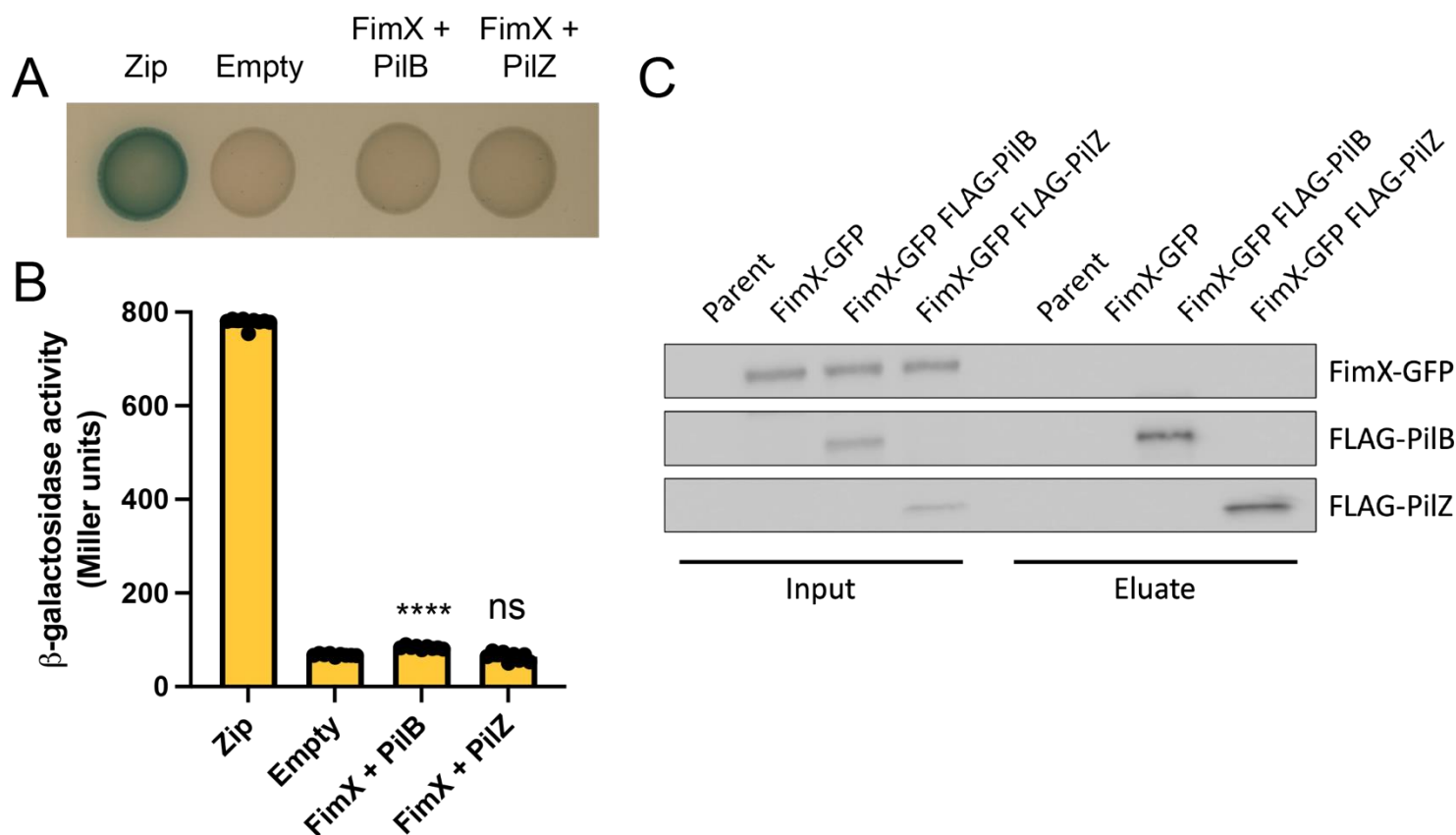703 e03754-21.

704

Figure 1

Figure 1. FimX does not interact with PilB nor PilZ in *A. baylyi.* A) BACTH interactions between FimX and PilB/PilZ fused N-terminally to the T25 and T18 domains of adenylate cyclase, respectively, following incubation at 30 °C for 48 hours and subsequently at 4 °C for 24 hours on LB agar plates containing X-Gal. Leucine zipper motif (zip) fused to T18 and T25 was used as positive control while empty vectors of T18 and T25 alone (empty) was the negative control. B) Quantification of β-galactosidase activity in Miller units for the same interactions depicted in A. The data show three biological replicates each with three technical replicates. Error bars show mean ± SD and statistical significance was determined using Dunnett's multiple comparisons test against the empty vector control. ****$p < 0.0001$. ns, not significant. C) Western blot showing coimmunoprecipitation experiments where 3xFLAG-PilB or 3xFLAG-PilZ was used as the bait protein to test for interaction with FimX-GFP as the prey protein. Blot was probed using both α-FLAG and α-GFP antibodies to detect both proteins simultaneously.
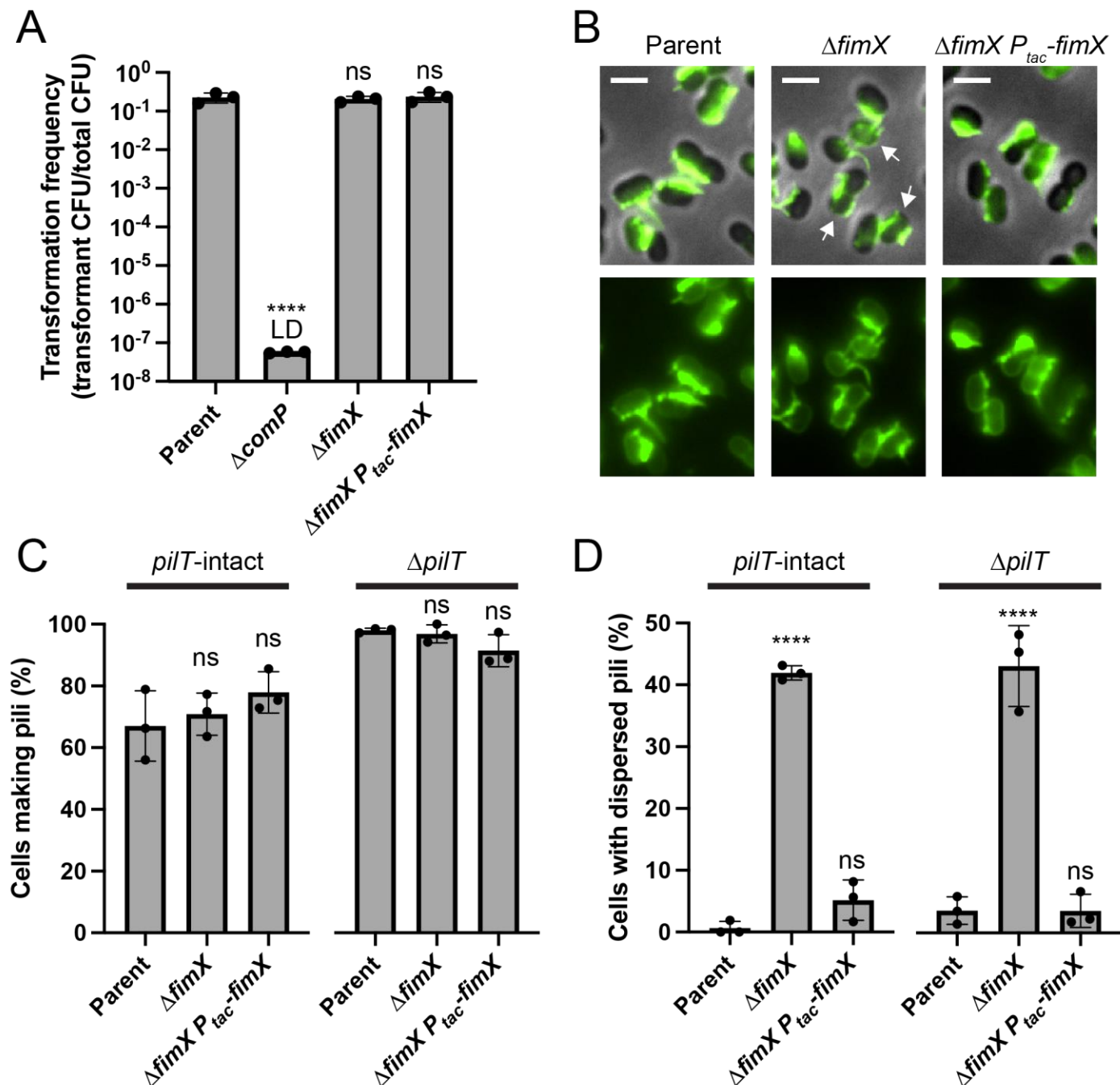
Figure 2

Figure 2. Deletion mutants of *fimX* make mislocalized T4P. A) Natural transformation assays of indicated strains. LD, limit of detection. Statistical significance was determined using log-transformed transformation frequencies. B) Representative microscopy images of indicated strains in a Δ*pilT* retraction motor deletion parent strain labeled with AF488-mal. Arrows indicate cells with mislocalized T4P. Scale bars, 2 μm. C) Percent of piliated cells in indicated strains. D) Percent of cells with mislocalized or dispersed T4P in indicated strains. Cells with dispersed T4P were defined as cells that had T4P on both long-axis sides of the cell body. For panels A,C,D, each data point represents a biological replicate (n = 3), and bar graphs indicate the mean ± SD. A minimum of 50 cells were analyzed per replicate. Statistical significance was determined using Dunnett's multiple comparisons test against the parent strain for each data set. ****$p < 0.0001$. ns, not significant.
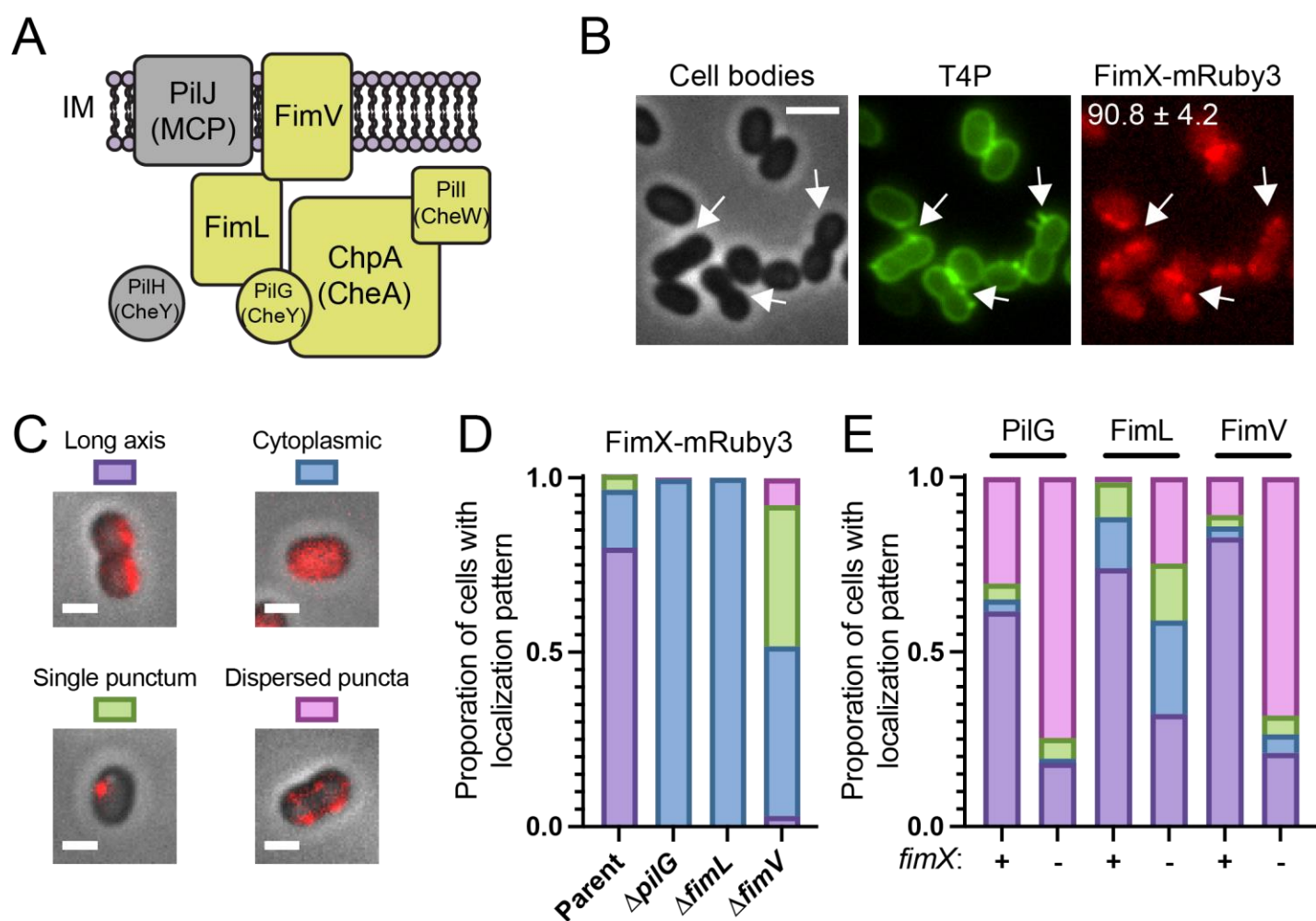
Figure 3. FimX is part of the Pil-Chp chemosensory system. A) Schematic of the Pil-Chp components found in *A. baylyi* with analogous flagellar chemotaxis protein names in parentheses. Deletions of components colored gold cause dispersed T4P localization while deletion of components in gray have no effect on localization of T4P. IM, inner membrane. B) Representative microscopy images of strain containing FimX-mRuby3 with AF488-mal labeled. Scale bar, 2 μm. Arrows indicate FimX-mRuby3 localizing to the base of T4P. Number in top right corner indicates the average percent of piliated cells that have FimX-T4P colocalization. C) Representative microscopy images of single cells with localization patterns quantified in D and E. Scale bars, 1 μm. D) Quantification of FimX-mRuby3 localization in indicated strains. E) Quantification of localization patterns of PilG-mRuby3, FimL-mCherry, or FimV-mRuby3 in the presence or absence of *fimX*. Data for D and E are shown as the average proportion of each localization pattern shown in C from three biological replicates. A minimum of 50 total cells were assessed for each biological replicate.
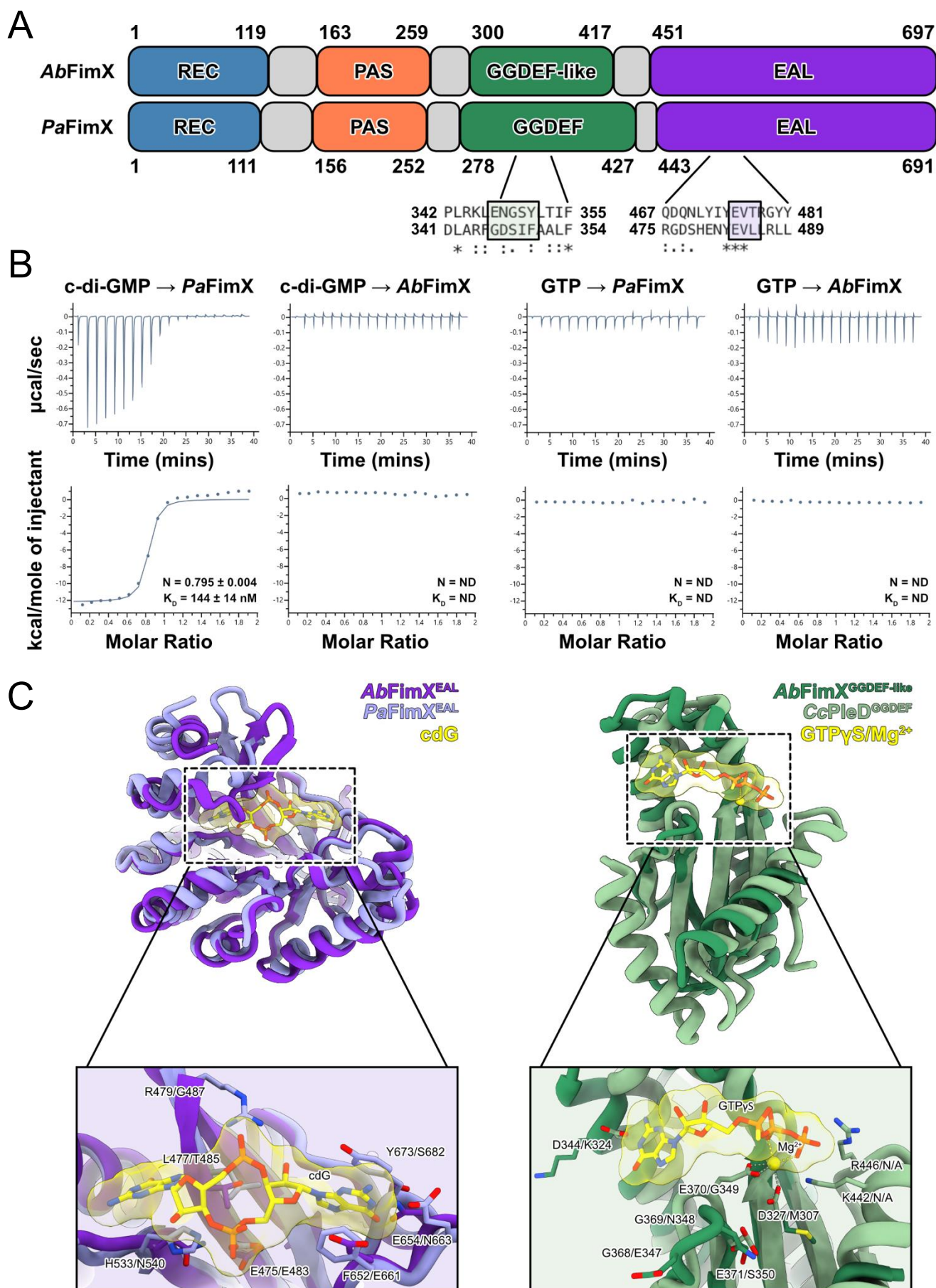
Figure 4

Figure 4. *A. baylyi* FimX does not bind cdG nor GTP. A) Schematic of *A. baylyi* (*Ab*FimX) and *P. aeruginosa* (*Pa*FimX) FimX domain organization from Foldseek and AlphaFold3 modeling. In *Ab*FimX, the blue region encompasses a receiver domain (REC); orange region encompasses a Per-ARNT-Sim (PAS) domain; green region encompasses a GGDEF-like domain; purple region encompasses a phosphodiesterase domain (EAL). Black-boxed region shows sequence alignment of the degenerate GGDEF and EAL motifs between *Ab*FimX and *Pa*FimX. B) Calorimetric titrations of 250 µM cdG or 1 mM GTP into 25 µM or 100 µM *Pa* and *Ab* FimX, respectively. Top panel depicts the heat release from injections while the bottom panel shows the normalized fitted binding curve. The stoichiometry (N) and the dissociation constant (KD) are displayed if binding was observed. ND, not determined. C) (left) Superimposition of the crystal structure of the cdG-bound EAL domain from *Pa*FimX (light purple) (PDB: 3HV8) onto the AlphaFold3 predicted EAL domain of *Ab*FimX (dark purple). Bottom panel depicts the close-up view of the active site with residues in *Pa*FimX involved in cdG binding shown on the left and equivalent residues that diverged in *Ab*FimX highlighted on the right. (right) Superimposition of the crystal structure of the GTPγS-bound GGDEF domain from *Caulobacter crescentus* PleD (*Cc*PleD) (light green) (PDB: 2V0N) onto the AlphaFold3 predicted GGDEF-like domain of *Ab*FimX (dark green). Bottom panel depicts the close-up view of the nucleotide binding pocket with residues in *Cc*PleD involved in GTPγS/Mg^{2+} binding shown on the left and equivalent residues that diverged in *Ab*FimX depicted on the right.
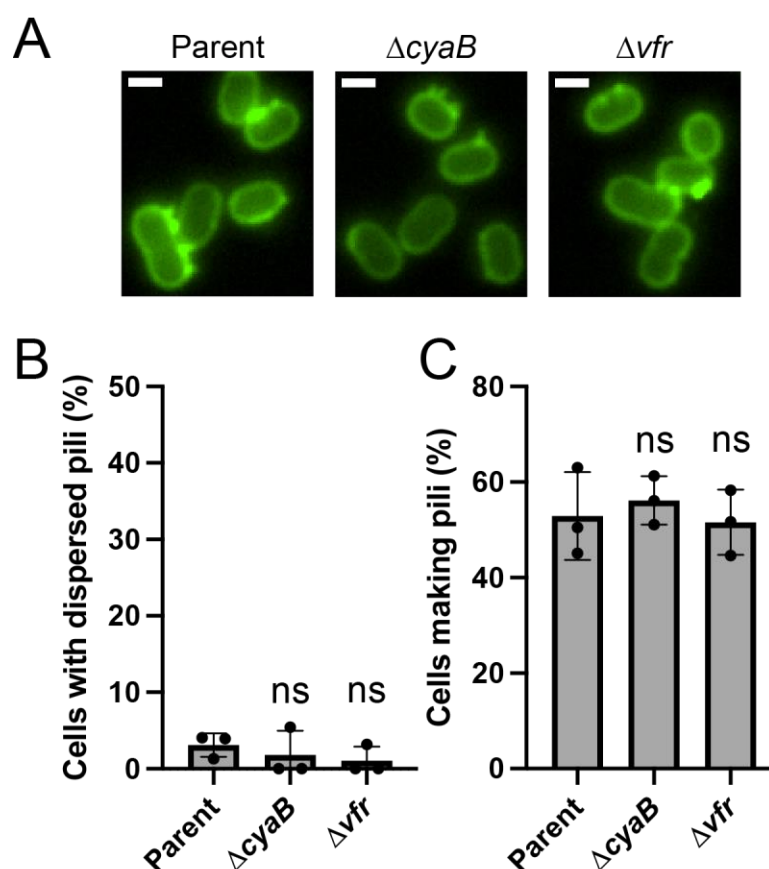
Figure 5

Figure 5. cAMP signaling factors do not influence T4P production nor localization. A) Representative microscopy images of indicated strains labeled with AF488-mal with background fluorescence subtracted. Scale bars, 1 μm. B) Percent of cells with mislocalized or dispersed T4P in indicated strains. C) Percent of piliated cells in indicated strains. Each data point represents a biological replicate (n = 3), and bar graphs indicate the mean ± SD. A minimum of 50 cells were analyzed per replicate. Statistical significance was determined using Dunnett's multiple comparisons test against the parent strain for each data set. ns, not significant.
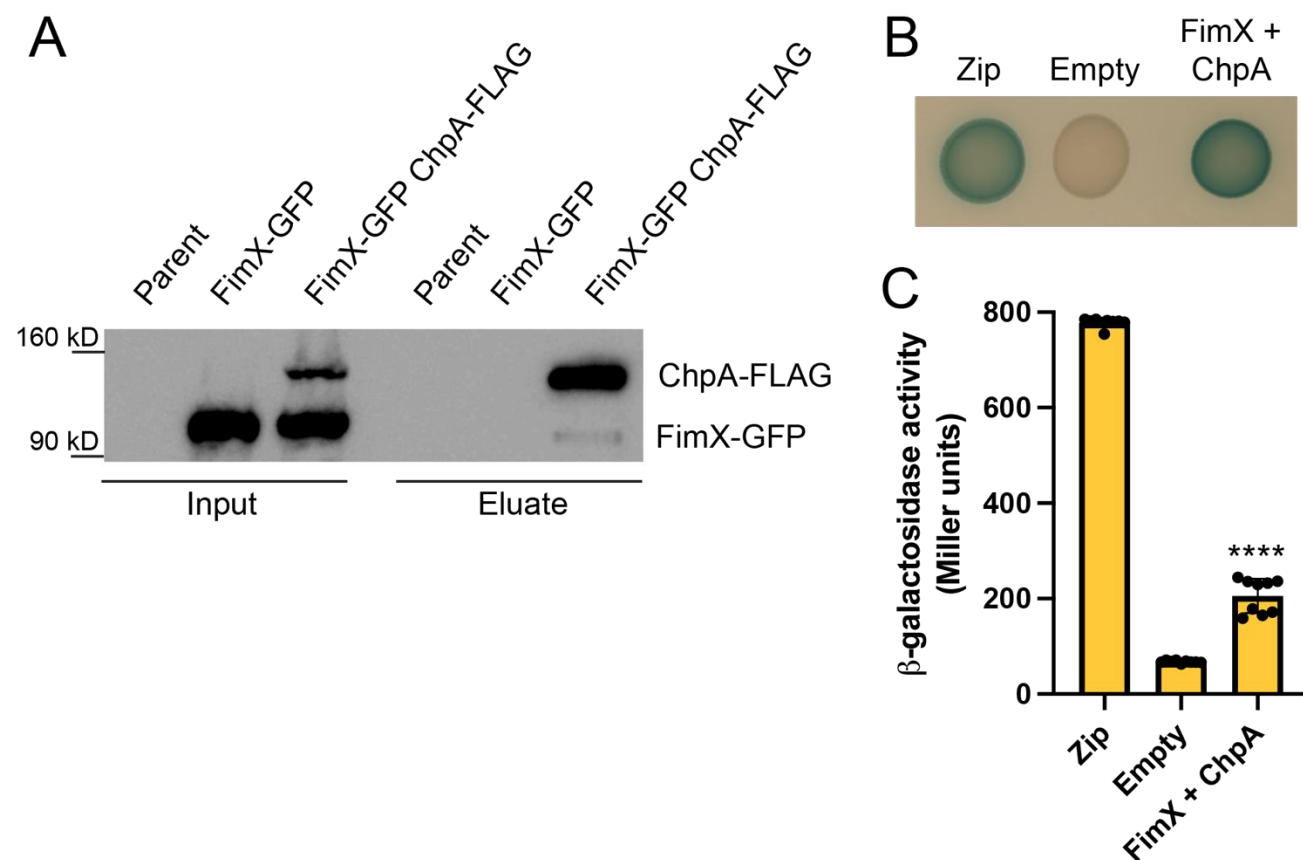
Figure 6

Figure 6. FimX directly interacts with ChpA. A) Western blot showing coimmunoprecipitation experiments where ChpA-FLAG was used as the bait protein to test for interaction with FimX-GFP as the prey protein. The blot was probed using both α-FLAG and α-GFP antibodies to detect both proteins simultaneously. B) BACTH interaction between FimX and ChpA fused N-terminally to the T25 and T18 domains of adenylate cyclase, respectively, following incubation at 30 °C for 48 hours and subsequently at 4 °C for 24 hours on LB agar plates containing X-Gal. Leucine zipper motif (zip) fused to T18 and T25 was used as positive control while empty vectors of T18 and T25 alone (empty) was the negative control. C) Quantification of β-galactosidase activity in Miller units for the same interactions depicted in B. The data show three biological replicates each with three technical replicates. Error bars show mean ± SD and statistical significance was determined using Dunnett's multiple comparisons test against the empty vector control. ****$p < 0.0001$.